DOI: 10.1002/ejic.200700939

Immobilisation of η^3-Allyldicarbonyl Complexes of Mo^{II} with Bidentate Nitrogen Ligands within Aluminium-Pillared Clays

João Carlos Alonso,[a] Patrícia Neves,[b] Carlos Silva,[b] Anabela A. Valente,[b] Paula Brandão,[b] Susana Quintal,[c] Maria J. Villa de Brito,[c,d] Patrícia Pinto,[e] Vítor Félix,[b] M. G. B. Drew,[f] João Pires,[c] Ana Paula Carvalho,[c] Maria José Calhorda,[c] and Paula Ferreira*[a]

Keywords: Molybdenum complexes / N ligands / Clays / Epoxidation

Molybdenum(II) complexes $[MoX(CO)_2(\eta^3\text{-allyl})(CH_3CN)_2]$ (X = Cl or Br) were encapsulated in an aluminium-pillared natural clay or a porous clay heterostructure and allowed to react with bidentate diimine ligands. All the materials obtained were characterised by several solid-state techniques. Powder XRD, and ^{27}Al and ^{29}Si MAS NMR were used to investigate the integrity of the pillared clay during the modification treatments. ^{13}C CP MAS NMR, FTIR, elemental analyses and low-temperature nitrogen adsorption showed that the immobilisation of the precursor complexes was successful as well as the in situ ligand-substitution reaction. The new complex $[MoBr(CO)_2(\eta^3\text{-allyl})(2\text{-aminodipyridyl})]$ was characterised by single-crystal X-ray diffraction and spectroscopic techniques, and NMR studies were used to investigate its fluxional behaviour in solution. The prepared materials are active for the oxidation of *cis*-cyclooctene using *tert*-butyl hydroperoxide as oxidant, though the activity of the isolated complexes is higher.

Introduction

In the last decade much research has been carried out aimed at developing a new class of materials named pillared interlayered clays (PILCs), which seem to be promising supports for organometallic catalysts. The PILCs are prepared from cationic clays by exchanging the interlayered cations with large polyoxo and polyoxy cations. After calcination, the polyoxo and polyoxy cations are converted into metal oxide clusters, creating a regular structure running in two directions with an interlayer spacing able to accommodate molecular entities.[1,2]

More recently other types of porous materials where prepared from clay minerals, which have been referred to as "porous clays heterostructures" (PCHs).[3] These solids differ from PILCs in the sense that the clay layers are firstly expanded by long-chain cationic (surfactant) species and later, with the help of long-chain amines as cosurfactants, permanent porosity is formed by the polymerisation of organosilica sources.[3,4] The PCHs can be applied in the design of heterogeneous catalysts, bridging an important pore-size region between microporous zeolites and pillared clays (<10 Å) and the M41S mesoporous materials (>20 Å). Besides the size of the pores, the nature of the pillars (oxides vs. silicates) is also different, leading to more diverse reactivity.

There are very few reports on the encapsulation of transition-metal complexes into pillared clays using different methodologies. Both copper(II) acetylacetonate and manganese(III) salen complexes could be encapsulated simultaneously with the pillaring formation process of a montmorillonite clay with aluminium polyoxycations.[5,6] Manganese(III) salen complexes were immobilised into pillared clays by a two-step methodology that consisted of the adsorption of a precursor metal complex in the PILC followed by diffusion of the ligands.[7,8] All these materials were efficient catalysts in the epoxidation of styrene at room temperature, using PhIO as oxygen source and acetonitrile as solvent.

Recently, we found that complexes of the type $[MoX(CO)_2(\eta^3\text{-allyl})(N\text{–}N)]$, with N–N = $(CH_3CN)_2$ or diimine ligands, were quite active and very selective catalyst

[a] Departamento de Engenharia Cerâmica e do Vidro, CICECO, Universidade de Aveiro,
Campus Universitário de Santiago, 3810-193 Aveiro, Portugal
Fax: +351-234370204
E-mail: pcferreira@ua.pt
[b] Departamento de Química, CICECO, Universidade de Aveiro, Campus Universitário de Santiago, 3810-193 Aveiro, Portugal
[c] Departamento de Química e Bioquímica, CQB, Faculdade de Ciências, Universidade de Lisboa, Ed. C8, Campo Grande, 1749-016 Lisboa, Portugal
[d] Centro de Química Estrutural, Instituto Superior Técnico, Av. Rovisco Pais, 1049-001 Lisboa, Portugal
[e] Instituto de Tecnologia Química e Biológica, Av. da República, EAN, Apart. 127, 2781-901 Oeiras, Portugal
[f] Department of Chemistry, University of Reading, Whiteknights, Reading RG6 6AD, UK

precursors for olefin epoxidation using *tert*-butyl hydroperoxide (TBHP) as oxygen donor, without co-solvent, at 328 K.[9] The results obtained in two consecutive catalytic runs were quite similar. Nevertheless, these catalytic systems can suffer from well known drawbacks of homogeneous catalytic processes. In the present work, we set out to immobilise η^3-allyldicarbonyl molybdenum(II) complexes in microporous ordered aluminium pillared clays, using a two-step methodology consisting of the intercalation of $[MoX(CO)_2(\eta^3\text{-}C_3H_5)(CH_3CN)_2]$, with X = Br (**1**), Cl (**2**), followed by reaction with the bidentate ligands di(2-pyridyl)amine (**adp**) or 1,4-bis(2,6-dimethylphenyl)-2,3-dimethyl-1,4-diazabutadiene (**dab**). A PCH material was prepared and used as an alternative support for immobilising the organometallic complexes because of its larger specific surface area. The supported materials have been characterised by elemental analysis, powder X-ray diffraction (XRD), N_2 adsorption studies, FTIR and solid-state magic angle spinning (MAS) NMR (^{13}C, ^{27}Al, ^{29}Si) spectroscopy. The catalytic properties of the materials were investigated in the epoxidation of cyclooctene using TBHP as oxygen source.

Results and Discussion

A new derivative of the $Mo^{II}X(\eta^3allyl)(CO)_2$ fragment with the nitrogen bidentate ligand **adp** was synthesised from the precursor complex $[MoBr(CO)_2(\eta^3\text{-}C_3H_5)(CH_3CN)_2]$, **1**, by substitution of two nitrile ligands (Scheme 1) in ethanol.

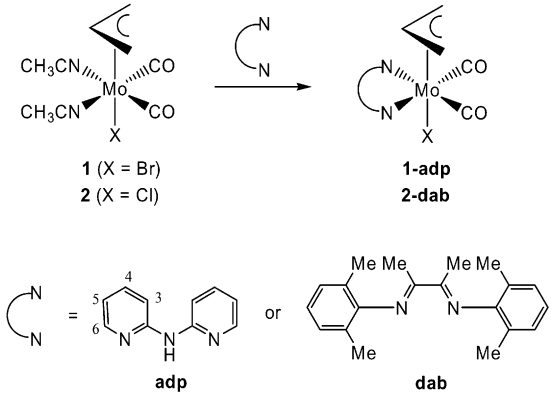

Scheme 1.

The molecular structure of the complex $[MoBr(CO)_2(\eta^3\text{-}C_3H_5)(adp)]$ (**1-adp**) determined by single-crystal X-ray diffraction is shown in Figure 1 with the atomic notation scheme. Selected bond lengths and angles are listed in Table 1.

The molybdenum centre exhibits a pseudo-octahedral coordination environment with the centroid of η^3-allyl ligand and two carbonyl ligands determining a *fac* arrangement. The **adp** ligand is coordinated in a bidentate chelating fashion, with Mo–N distances of 2.289(6) and 2.291(6) Å, and a chelating angle of 87.0(3)°. Furthermore, the two pyridine rings are bent by 23.5(2)° relative to the N–H bridging

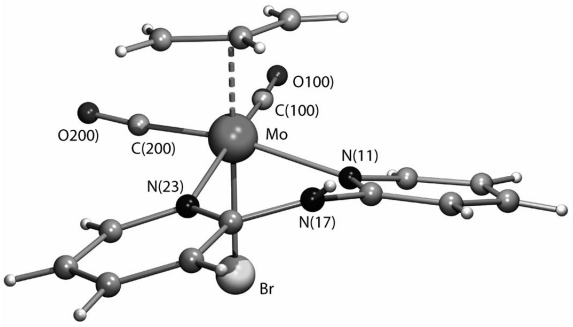

Figure 1. Molecular structure of $[MoBr(CO)_2(\eta^3\text{-}C_3H_5)(adp)]$ (**1-adp**).

Table 1. Bond lengths (Å) and angles (°) subtended at the molybdenum(II) centre.

Mo–C(200)	1.950(9)	Mo–C(100)	1.960(10)
Mo–N(11)	2.289(6)	Mo–N(23)	2.291(6)
Mo–Br	2.669(1)		
C(100)–Mo–C(200)	76.4(3)	N(11)–Mo–N(23)	81.5(2)
C(100)–Mo–N(11)	167.2(3)	C(200)–Mo–N(11)	100.4(3)
C(100)–Mo–N(23)	99.6(3)	C(200)–Mo–N(23)	170.2(3)
C(100)–Mo–Br	86.6(3)	C(200)–Mo–Br	89.2(3)
N(11)–Mo–Br	80.9(2)	N(23)–Mo–Br	81.6(2)

group. The values of these structural parameters are similar to those found for the octahedral complex $[Mo(CO)_4(adp)]$[10] with average Mo–N distances of 2.274 Å, and a N–Mo–N angle of 81.9°. The dihedral angle between the two aromatic rings is 22.9°. The complex coordination sphere is completed with Br in an axial position, 2.6692(10) Å from the metal centre, giving rise to the equatorial isomer depicted in Scheme 2. In the solid state, the allyl ligand adopts an *endo* conformation as shown in Figure 1. Equivalent geometric arrangements have been found in other related $Mo^{II}(\eta^3\text{-}C_3H_5)$ complexes, namely $[MoBr(CO)_2(\eta^3\text{-}C_3H_5)(N\text{–}N)]$, with N–N = 2,2′-bipyridyl, 4,4′-Me_2-2,2′-bipyridyl or *o*-phenanthroline.[11,12]

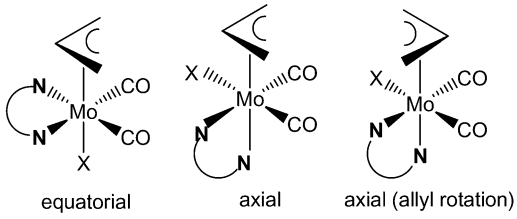

Scheme 2.

The crystal packing diagram presented in Figure 2 shows that in the solid state discrete molecules of **1-adp** self-assemble in 1D dimensional chains through N–H···Br hydrogen-bonding interactions, with H···Br distances of 2.729 Å and N–H···Br angles of 139°.

The infrared spectrum of $[MoBr(\eta^3\text{-}C_3H_5)(CO)_2(adp)]$ (**1**) showed the two $\nu_{C\equiv O}$ stretching bands of the carbonyl groups at 1929 and 1840 cm^{-1}, as well the ν_{N-H} stretching at 3280 cm^{-1}, and two bands at 1634 and 1583 cm^{-1}, as-

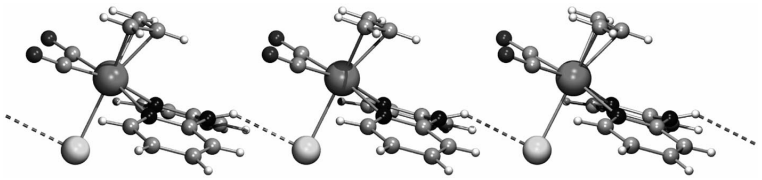

Figure 2. Crystal packing diagram of **1-adp** showing the chain of $[MoBr(CO)_2(\eta^3\text{-}C_3H_5)(adp)]$ molecules in one dimension, assembled by N–H···Br bonds.

signed to $\nu_{C=N}$ vibrations of the coordinated pyridine rings. The characteristic bands of the nitrile were absent, indicating that these ligands had been substituted.

The ^{1}H NMR spectrum of complex **1-adp** at room temperature showed broad resonances and three peaks at 10.57, 10.88 and 11.15 ppm, assigned to the NH protons, indicating the presence of three isomers (Scheme 2) and fluxional behaviour in solution. An ^{1}H NMR variable-temperature study (Figure 3) shows that at lower temperatures the interchange processes are slower and at 233 K the proton signals split and the spectrum exhibits three sets of resonances with integration ratios of 1.0:0.3:0.1, confirming the coexistence of three isomers. ^{13}C, 2D ^{1}H COSY and phase-sensitive 2D ^{1}H NOESY spectra have also been recorded at 233 K.

The set of resonances corresponding to the main isomer A is typical of symmetrical η^3-allyl complexes (equatorial, Scheme 2), with the A_2B_2X spin pattern for the allyl moiety (a triplet of triplets, although not totally resolved, at δ = 4.05 ppm, and two doublets at δ = 2.44 and 1.14 ppm, assigned to the *meso*, *syn* and *anti* protons, respectively) and four resonances for the protons of the equivalent **adp** rings (two doublets at δ = 8.37 and 7.24 ppm, and two triplets at δ = 7.87 and 7.24 ppm, assigned to protons $H_{6,6'}$, $H_{3,3'}$, $H_{4,4'}$ and $H_{5,5'}$, respectively). The NOE correlation indicates a close spatial proximity of the *syn* protons to the allyl ligand and $H_{6,6'}$ of the **adp** ligand, which is in agreement with the X-ray data found for the equatorial isomer in the solid-state structure described above.

The sets of resonances assigned to isomers B and C show the ABCDX spin pattern for the allyl moiety and the nonequivalence of the two pyridine rings of the **adp** ligand, which are characteristic of asymmetric allylic complexes (axial, Scheme 2). The NOESY spectrum shows that the *meso* protons of B and C (4.16 and 4.24 ppm, respectively) are both correlated to two aromatic protons of the corresponding **adp** ligands. The shift to higher frequencies of the N**H** resonances of the three isomers as the temperature is lowered (Figure 3) is indicative of a higher degree of intermolecular H-bonding, which is in agreement with what is observed in the solid-state structure (see Figure 2). The absence of negative cross-peaks in the NOESY spectrum indicates that no chemical exchange occurs at low temperature. These spectroscopic data support the coexistence, in solution, at low temperature, of an equatorial and two axial isomers. The equatorial isomer corresponds to the solid-state structure, as discussed above, and can transform into the axial one by a trigonal twist mechanism.[11,13,14] While the equatorial isomer has a symmetry plane, the axial one has no symmetry, and five different chemical shifts, instead of three, can be expected for the allyl protons; the two pyridine rings are also nonequivalent. A third isomer, shown in Scheme 2 (right), is obtained by allyl rotation of B and is the most likely one for isomer C.

The complexes $[MoX(CO)_2(\eta^3\text{-}C_3H_5)(CH_3CN)_2]$, **1** (X = Br) and **2** (X = Cl), were first introduced using an impregnation process by dipping the PILC in solutions of com-

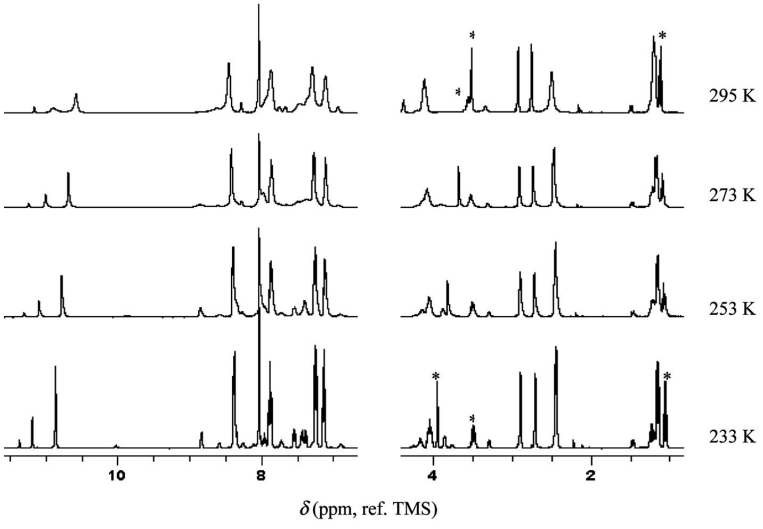

Figure 3. Variable-temperature ^{1}H NMR spectra of **1-adp** in $[D_7]$DMF showing the NH, the aromatic and the allyl regions (* indicates impurity signals; diethyl ether included).

plexes **1** or **2** in acetonitrile at room temperature, as represented in Scheme 3. After 40 h of stirring, the complexes **1** or **2** impregnated into the PILC were allowed to react with an excess of either **adp** or **dab** ligand (Scheme 1) to promote the in situ substitution of the labile acetonitrile ligands, affording the materials PILC/**1-adp**, PILC/**2-adp** and PILC/**2-dab**. Complex **1** was also immobilised into a porous clay heterostructure (PCH) for comparison. The addition of the **adp** ligand led to the final material (PCH/**1-adp**).

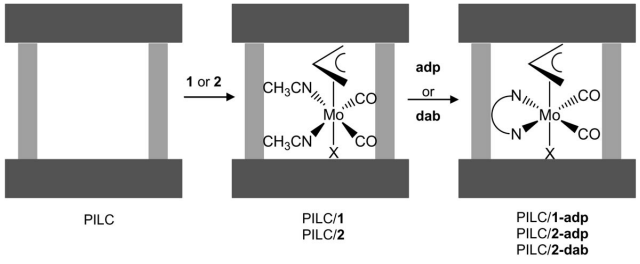

Scheme 3.

The corresponding complexes **1-adp** and **2-dab** were prepared for comparison with the composite materials. The complexes of $[MoX(CO)_2(\eta^3\text{-}C_3H_5)(CH_3CN)_2]$ with **adp** and **dab** exhibit different structures in the solid state, corresponding to the two possible isomers, axial and equatorial (Scheme 2). While $[MoX(CO)_2(\eta^3\text{-}C_3H_5)$(**dab**)] remains as a single axial isomer in solution, as in the solid state,[9] the **adp** derivative occurs in the solid as the equatorial isomer (Figure 1).

The powder XRD pattern of the PILC (Figure 4) shows only a broad band centred at about $2\theta = 4.84°$ corresponding to a basal spacing d_{001} of 1.82 nm. The structure and basal spacing of the PILC remain unchanged after the encapsulation of the Mo^{II} complexes, as can be observed for the modified materials (Figure 4). In the PCH materials, it was not possible to detect an X-ray diffraction pattern at low angles when using either oriented or nonoriented mounts. This observation may be related with poor long-range order.[4,15]

Low-temperature nitrogen adsorption and desorption isotherms of the PILC, PCH and modified materials are presented in Figure 5. A similar profile between the pristine and modified materials can be observed. The isotherms of the functionalised PILC and PCH samples show a lower N_2 initial uptake, leading to a decrease in the specific surface areas (A_{BET}) (Table 2). As can be noticed from Figure 5, below relative pressures of 0.2, where the adsorption occurs in the micropores (widths lower than 2 nm as defined by the IUPAC), the adsorbed amount in PILC/**1** is lower than in the pristine PILC. This is consistent with the decrease of the specific surface area values given in Table 2. In the multilayer region, for relative pressures higher than 0.4 (Figure 5), the N_2 adsorbed amount in PILC/**1** is higher than in PILC. In this portion of the isotherm, the adsorption proceeds in the external surface of the crystallites and/or in some type of mesoporosity. In PILCs, the mesoporosity usually results from the aggregation of the clay. Therefore, this may indicate that during the immobilisation of complex **1** into the PILC in the presence of the organic solvent, the clay particles aggregate in a different way.

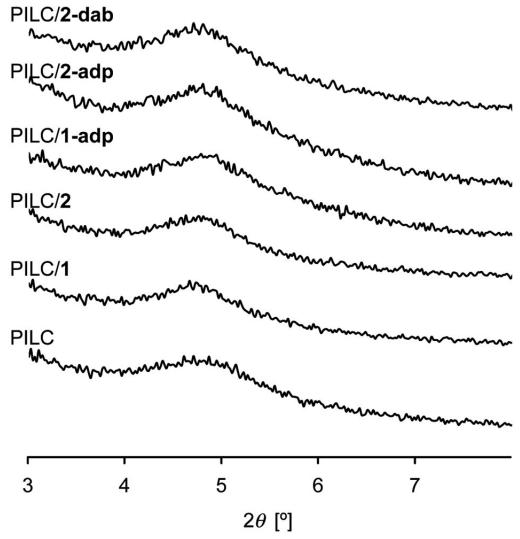

Figure 4. Powder XRD patterns of the parent and modified PILCs.

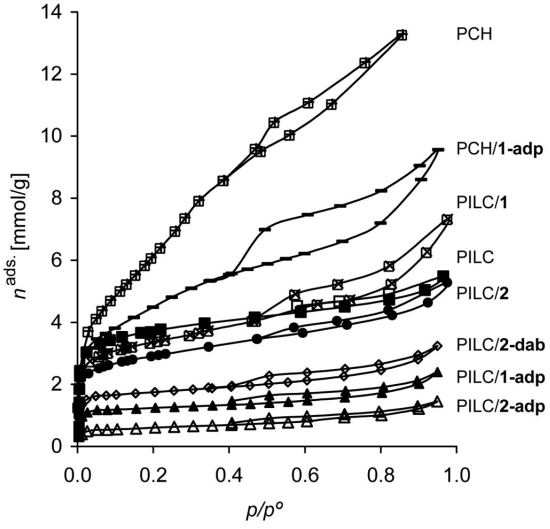

Figure 5. Nitrogen adsorption–desorption isotherms at 77 K of the parent and modified materials.

Table 2. Mo content and textural parameters for pristine and functionalised materials taken from N_2 adsorption data collected at 77 K.

Material	Mo wt.-%	A_{BET} $m^2 g^{-1}$	ΔA_{BET}[a] %	V_{micro} $cm^3 g^{-1}$	V_{meso} $cm^3 g^{-1}$
PILC		277	–	0.12	0.06
PILC/**1**	1.4	268	–3	0.08	0.18
PILC/**2**	1.4	231	–17	0.08	0.10
PILC/**1-adp**	2.25	95	–66	0.03	0.05
PILC/**2-adp**	2.68	60	–78	0.02	0.04
PILC/**2-dab**	0.80	113	–59	0.03	0.10
PCH		493	–	0.19	0.27
PCH/**1-adp**	2.55	295	–40	0.07	0.23

[a] Variation of surface area in relation to parent material.

The values of A_{BET} decrease further after the addition of the dinitrogen ligands. The reduction of the surface area is proportional to the molybdenum loading in almost all cases. The metal content may be dependent on the size of the complex and ligand, and on the stereoisomer preferentially formed. For the PILC/**2-dab** material, containing the axial isomer of the complex, a significant reduction of the A_{BET} (58%) is observed, but only 0.80 wt.-% of molybdenum was retained in the support. This observation, together with the value of carbon content determined by elemental analysis (3.45 wt.-% C), which was higher than the expected value (about 2.13 wt.-% C), suggests that PILC/**2-dab** contains a certain amount of free and/or decomposed **dab** molecules. The use of the PCH as support material led to a decrease of 40% of A_{BET}. The higher A_{BET} and higher pore volumes of the PCH in relation to the PILC did not significantly affect the total amount of supported Mo species (2.25 and 2.55 wt.-% Mo for PILC/**1-adp** and PCH/**1-adp**, respectively). The retention of the complexes inside the PILC or PCH materials seems to occur preferentially at the micropores, with consequent reduction of their volume (Table 2).

FTIR spectra (not shown) were recorded before and after immobilisation of the complexes. All solids present the two typical C≡O stretches of the complexes (Table 3); in the case of PILC/**2-dab**, these bands are very weak. The observation of the C≡O stretches in all the functionalised clays proves that the immobilisation of the complexes into the PILC was successful, as these bands are the strongest and the more reliable to identify carbonyl complexes. The slight shifts in relation to the frequency of the C≡O stretches in the corresponding precursor complexes **1**, **2**, **1-adp** and **2-dab** reflect the small changes in electron density at the metal derived from the interaction with the surface of the clay.

Table 3. FTIR wavenumbers of the $\nu_{C\equiv O}$ modes of the functionalised materials and the corresponding complexes (in parentheses).

Material	$\nu_{C\equiv O}$ [cm^{-1}]
PILC/**1**	1934, 1830 (1949, 1851)
PILC/**2**	1937, 1834 (1941, 1851)
PILC/**1-adp**	1929, 1839 (1927, 1841)
PILC/**2-adp**	1926, 1840
PCH/**1-adp**	1930, 1843 (1927, 1841)
PILC/**2-dab**	1953, 1868 (1938, 1847)

The ^{29}Si MAS NMR spectra of the materials are shown in Figure 6. The ^{29}Si MAS NMR spectrum of the PILC shows only one peak at –94.1 ppm. The observed peak was assigned to a Q^3 environment, that is, silicon in a tetrahedral sheet having an Al neighbour, $Si(OSi)_3Al$. No $Si(OSi)_{4-x}(OH)_x$ environments were identified. The ^{29}Si MAS NMR spectra of the modified PILCs are comparable to the spectrum of the parent PILC, indicating that the basic pillared structure was not destroyed by the encapsulation of the complexes. Many spinning side bands were observed, which can be related to the presence of paramagnetic Fe^{3+} species in the clay.

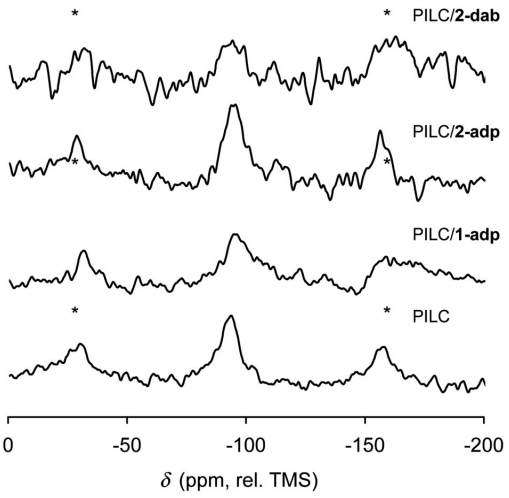

Figure 6. ^{29}Si MAS NMR spectra of the parent PILC, PILC/**1-adp**, PILC/**2-adp** and PILC/**2-dab** recorded at 5 kHz.

The ^{13}C CP MAS spectra of complexes **1** and **1-adp**, and materials PILC/**1-adp**, PCH/**1-adp** and PILC/**2-adp** are shown in Figure 7. The spectrum of complex **1** exhibits one peak at $\delta \approx 124$ ppm, attributed to Me**C**N, and one peak at $\delta \approx -6.0$ ppm, attributed to **Me**CN. The peaks at $\delta \approx 53$ and 72 ppm are assigned to $\mathbf{C}_{allyl–anti/syn}$ and $\mathbf{C}_{allyl–meso}$, respectively. The C≡O resonance appears at $\delta \approx 223$ ppm. When the acetonitrile ligands are replaced by the **adp** ligand to form complex **1-adp**, the signals assigned to the acetonitrile ligands disappear and a set of new peaks can be observed. The spectrum of complex **1-adp** exhibits peaks at $\delta \approx 55.5$ and 68.6 of the allylic carbons; at 114.7, 117.2, 140.0 and 152.4 ppm of the aromatic carbons; and at $\delta = 224.1$ ppm assigned to the carbon of the carbonyl group. The spectra of PILC/**1-adp**, PCH/**1-adp** and PILC/**2-adp** provide clear evidence of the integrity of the complexes after the immobilisation process as all resonances are still present.

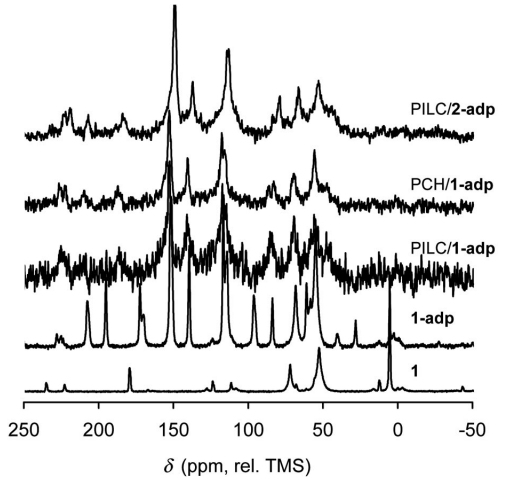

Figure 7. ^{13}C CP MAS NMR spectra of complexes **1** and **1-adp** and materials PILC/**1-adp**, PCH/**1-adp** and PILC/**2-adp** recorded at 7 kHz.

Figure 8 shows the ^{13}C CP MAS of complexes **2** and **2-dab**, and of material PILC/**2-dab**. Complex **2** displays two peaks at $\delta \approx 5.7$ and 123 ppm, assigned, respectively, to the resonances of the **Me**CN and Me**C**N of the acetonitrile ligands. The peaks at $\delta \approx 58.4$ and 70.1 ppm are attributed to the allyl groups, and the peak at $\delta \approx 223$ ppm is the resonance of the carbonyl. The spectrum of complex **2-dab** shows the expected peaks of the **dab** ligand at $\delta \approx 20.4$ ppm for the methyl groups; at $\delta \approx 126.4$, 128.2, 129.3 and 149.0 ppm for the aromatic carbons and at $\delta \approx 174$ ppm for **C**=N. The spectrum of PILC/**2-dab** is not well resolved although many scans were required to obtain this pattern. The broad peak at $\delta = 130$ ppm suggests that the aromatic rings are present. A possible explanation for the poor quality of the spectrum is the existence of different steric constraints of the complex, associated with the bulk of the ligand and the presence of the axial isomer, which force it to be too close to the paramagnetic centres of the PILC material, which would result in broad signals. On the other hand, as suggested above, some free and/or decomposed **dab** is possibly present in the PILC support, which may lead to many different chemical environments of carbon inside the clay, giving rise to a poor-quality spectrum. It was not possible to detect the ^{13}C CP MAS spectra of PILC/**1** and PILC/**2** materials.

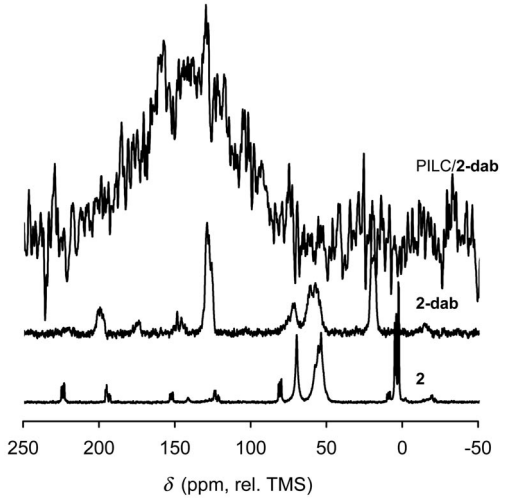

Figure 8. ^{13}C CP MAS NMR spectra of complexes **2** and **2-dab** and material PILC/**2-dab** recorded at 7 kHz.

The clay-supported complexes prepared in this work were tested as catalyst precursors for the liquid-phase epoxidation of *cis*-cyclooctene (chosen as model compound), using *tert*-butyl hydroperoxide (TBHP) as oxygen donor, without additional solvent, at 328 K. For comparison, complexes **1**, **2**, **1-adp** and **2-dab** were tested as homogeneous catalysts, under similar reaction conditions. In the presence of the pristine PILC, the reaction is sluggish and poorly selective to 1,2-cyclooctane oxide (59% at 18% conversion, at 24 h), yielding the corresponding diol as by-product (Table 4). The PILC/**dab** material (without Mo) gives 18% conversion at 24 h and 55% epoxide selectivity, whereas PILC/**2-dab** gives 41% conversion and 100% selectivity. When a Mo-containing catalyst is used without TBHP, no reaction occurs, in contrast to what is observed with TBHP, indicating that the hydroperoxide is necessary for the formation of active oxidising species. It has been reported for (cyclopentadienyl)$Mo(CO)_3Cl$-type compounds, used as catalyst precursors for cyclooctene epoxidation under similar reaction conditions, that the oxidative decarbonylation (OD) of the complexes with TBHP is necessary for the formation of active oxomolybdenum species.[16,17] A similar mechanistic feature may be involved for the compounds described above, as postulated in our recent work.[9] In general, no induction periods are observed for the carbonyl precursor complexes, suggesting that the OD is relatively fast and does not limit the rate of epoxidation of cyclooctene. In order to investigate if the oxidising species are Mo species and/or peroxide radicals derived from TBHP, the reaction of cyclooctene in the presence of **2** and PILC/**2** was performed using equimolar amounts of olefin and 2,6-di-*tert*-butyl-4-methylphenol, used as a radical scavenger (RS). For both materials conversion at 2 h decreased somewhat when the RS was added: from 95 to 80% for **2**, and from 3% to <1% for PILC/**2**, suggesting that the reaction is partly catalysed by free radicals, though to a much lower extent than by Mo species. When aqueous H_2O_2 is used instead of TBHP, the reaction in the presence of **2**, PILC/**2** and PILC/**2-adp** is very sluggish, giving 8%, 1% and 0% conversion at 4 h, in comparison to 97%, 4% and 34%, respectively, with TBHP. It has been reported for carbonyl complexes of the type (cyclopentadienyl)$Mo(CO)_3Cl$ that no catalytic epoxidation of olefins occurs when H_2O_2 is used as oxidant.[16]

Table 4. Cyclooctene epoxidation in the presence of bulk or supported Mo complexes, using TBHP as oxygen donor, at 328 K.

Compound	TOF[a] $mol\,mol_{Mo}^{-1}\,h^{-1}$	% Conversion[b] run 1/run 2	% Selectivity[b] run 1/run 2
PILC	<1	18	59
1	818	100:100	100:100
2	1089	100:100	100:100
1-adp	57	64:64	100:100
PILC/**1**	<1	10	88
PILC/**2**	<1	18	91
PILC/**1-adp**	31	60:63	100:100
PILC/**2-adp**	45	72:49	100:98
PCH/**1-adp**	21	61:58	100:100
2-dab	1134	97:87	100:100
PILC/**2-dab**	31	41:36	100:100

[a] Turnover frequency calculated at 10 min reaction. [b] Calculated for a first and second reaction run, at 24 h.

The kinetic profiles of the unsupported complexes **1** and **2** show a rapid increase in conversion during the first few minutes of reaction, leading to 100% epoxide yield within 6 h (Figure 9). The TOF is higher for **2** than for **1**, suggesting that the Cl ligand confers a higher reactivity to the complex than Br, without affecting selectivity (Table 4). The composites prepared using the **2** precursor also gave somewhat higher reaction rates than the corresponding materials

prepared using **1** (Table 4). Similar results have been reported previously for unsupported and silica-supported molybdenum complexes of the type MoO_2X_2L (X = Cl, Br; L is two monodentate or one bidentate neutral N-ligand).[18–22]

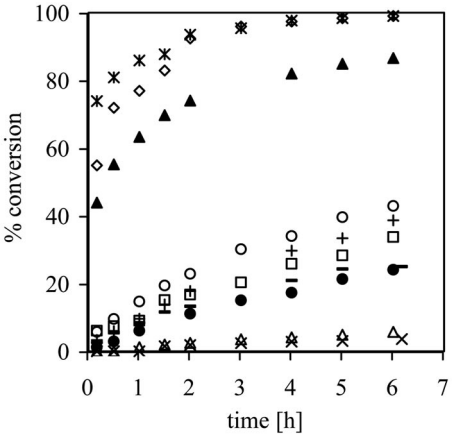

Figure 9. Kinetics profiles of cyclooctene epoxidation with TBHP, in the presence of **1** (✧), **2** (*), **1-adp** (□), **2-dab** (▲), PILC/**1** (×), PILC/**2** (△), PILC/**1-adp** (+), PILC/**2-adp** (○), PCH/**1-adp** (–) or PILC/**2-dab** (●), at 328 K.

The reaction rates for PILC/**1** and PILC/**2** are comparable to those observed for the pristine PILC, but epoxide selectivity is much higher (Table 4). The reaction is much slower for PILC/**1** and PILC/**2** than for their unsupported counterparts **1** and **2** (Figure 9, Table 4). According to the N_2 adsorption measurements, encapsulation of the complexes seems to take place preferentially inside the micropores of the clay support. Possibly the diffusion of the reactant molecules inside the clay structure is hindered and/or some active sites are inaccessible. However, most likely other factors are also responsible for the observed catalytic results, as the composites containing the chelating N ligands gave higher TOF than the corresponding PILC/**1** and PILC/**2** materials, as discussed later. It is also possible that the nature (structural and electronic features) of the supported metal species is different from that of the bulk complexes. The same reasoning applies to the active species generated from the supported Mo^{II} complexes in the presence of TBHP, which may be different when being formed on the support; furthermore, the active species may be generated more slowly on the clay support. The modification of metal precursors during immobilisation procedures has been reported for $MoO_2X_2(thf)_2$-type complexes, a variety of surface species being formed when attempting to immobilise these complexes on purely siliceous supports.[22]

The PILC/**1-adp** and PILC/**2-adp** materials give superior catalytic performances in relation to PILC/**1** and PILC/**2**, yielding 60–72% epoxide as the only product, at 24 h, while PILC/**1** and PILC/**2** give 8–17% epoxide plus up to 2% yield of the corresponding diol (Table 4). No major differences in catalytic activity are observed between PILC/**1-adp** and **1-adp** (Figure 9, Table 4). It seems that the introduction of chelating **adp** ligand during the synthesis procedure favours the formation of more active species than in the cases of PILC/**1** and PILC/**2**. For the clay/**1-adp** composites, the use of PCH as support instead of PILC does not influence product selectivity until 60% conversion, at least, and after 24 h both materials gave approximately the same amount of epoxide (Table 4). The main difference between the observed catalytic performances for these two materials is the slower reaction during the first 6 h for PCH/**1-adp** than for PILC/**1-adp** (used in the same weight) (Figure 9). Despite the slightly higher Mo loading and much higher A_{BET} of the former material, the powder XRD results suggest that PCH has poor long-range order, which may have a negative effect on catalytic activity (e.g. a fraction of active sites may be inaccessible to the relatively bulky olefin molecules because of partial pore blockage and/or steric hindrance).

When the bidentate ligand **dab** is used instead of **adp** to prepare PILC/**2-dab**, TOF is lower and the reaction is slower throughout 24 h in comparison to PILC/**2-adp**, which may be partly due to the lower amount of Mo species present in the former composite (0.80 and 2.68 wt.-% Mo for the **dab**- and **adp**-containing composite, respectively) (Figure 9). The reaction is much faster for **2-dab** than for PILC/**2-dab** (Figure 9, Table 4). The catalytic results obtained for PILC/**2-dab** are comparable to those reported in the literature for MCM-41- or MCM-48-supported complexes of the MoO_2X_2L family (L = 1,4-diazabutadiene ligand bearing triethoxysilyl groups), used as catalysts (with 1.0–1.4 wt.-% Mo) in the same reaction, under similar conditions.[23]

The unsupported complexes give practically the same conversions in two consecutive 24-h runs, revealing fairly high stability under the applied oxidising conditions (Table 4), as has been reported for similar species recently.[9] Similarly, the composite materials give comparable conversions when recycled (exemplified in Figure 10 for PILC/**1-adp**, and PCH/**1-adp**), with the exception of PILC/**2-adp**, which leads to a drop in conversion by a factor of 0.3. For PILC/**1-adp** and PILC/**2-adp** materials, ICP-AES analysis of the solids recovered after two runs indicated a reduction in the Mo content of 8–11%; in the cases of PILC/**1** and PILC/**2** it was less than 6%. Possibly, some metal species (on/closer to the external surface) that were not desorbed by the simple solvent extraction used in the catalyst preparation procedure could be desorbed under the applied reaction conditions. The hetero/homogeneous nature of the reaction was investigated for PILC/**1-adp** and PILC/**2-adp** by filtering the solids from the reaction solutions at 328 K, after 40 min, using a Whatman 0.2-μm (PVDF w/GMF) membrane, and leaving the solution to react for a further 320 min at 328 K. For both materials conversion increased by about 6% in the homogeneous phase, compared to about 33% in the presence of the solid catalysts. These results suggest that the catalytic reaction is mainly heterogeneous in nature, but there is also a catalytic contribution from the homogeneous phase. Despite the Mo leaching phenomenon, the enhanced catalyst deactivation observed

for PILC/**2-adp** may also result from the formation of some inactive molybdenum surface species during the epoxidation reaction.

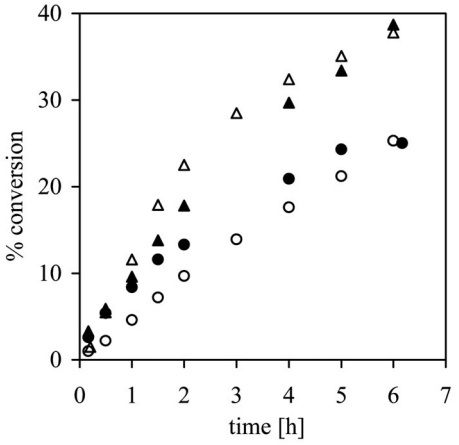

Figure 10. Cyclooctene conversion vs. time curves for PILC/**1-adp** (△) or PCH/**1-adp** (○), at 328 K, in a first (solid symbols) and second run (open symbols).

Conclusions

The immobilisation of the precursor complexes $[MoX(CO)_2(\eta^3\text{-allyl})(CH_3CN)_2]$ and their further reaction with chelating nitrogen ligands **adp** or **dab**, on PILC or PCH supports, was monitored by several techniques, namely FTIR, ^{29}Si, ^{27}Al and ^{13}C CP MAS NMR, and XRD. The clay structure was preserved during the post-synthesis treatments. The **adp** and **dab** complexes of the $MoX(CO)_2(\eta^3\text{-}C_3H_5)$ fragment display different structural preferences in the solid state. The smaller **adp** ligand leads to a more symmetric equatorial isomer in the crystal, exhibiting fluxional behaviour in solution. Low-temperature NMR studies showed the coexistence of three isomers, the equatorial one being the predominant species, along with two axial ones, differing by allyl rotation. The **dab** complex, on the other hand, prefers the asymmetric axial structure, probably owing to steric factors. The structural preferences may influence the behaviour of these complexes upon immobilisation. For example, the in situ **dab** ligand-substitution reactions can be constrained by steric factors due to the axial structural preference of this bulky ligand, which may partly account for the lower TOF observed for PILC/**2-dab** in comparison to **2-dab** and PILC/**2-adp** in the epoxidation of cyclooctene. The PILC/**1-adp** and PILC/**2-adp** materials gave superior catalytic performances in relation to PILC/**1** and PILC/**2**. The catalytic activities observed for the supported materials in olefin epoxidation were generally lower than for their unsupported counterparts. Most of the (un)supported materials prepared in this work gave roughly the same cyclooctene conversion at 24 h in two consecutive catalytic runs. The PILC seems to be a better support than PCH for supporting **1-adp**, leading to higher reaction rates. Hot-filtration tests carried out for the supported materials suggest that the catalytic reaction is mainly heterogeneous in nature, but there is also some catalytic contribution from the homogeneous phase (Mo leaching was less than 12% after two runs). More detailed characterisation studies of the materials before and after catalysis, or preferentially in situ characterisation techniques, could help understand better the observed differences in catalytic performances.

Experimental Section

Materials and Methods: All reagents were obtained from commercial sources and used as received. Solvents were dried using standard procedures (CH_2Cl_2 and CH_3CN over CaH_2), distilled under nitrogen and stored over 4-Å molecular sieves (3 Å for CH_3CN). 1,4-Bis(2,6-dimethylphenyl)-2,3-dimethyl-1,4-diazabutadiene (**dab**)[24] and the complexes $[MoBr(\eta^3C_3H_5)(CO)_2(CH_3CN)_2]$ (**1**), $[MoCl(\eta^3C_3H_5)(CO)_2(CH_3CN)_2]$ (**2**) and $[MoCl(\eta^3C_3H_5)(CO)_2\{(2,6\text{-}Me\text{-}C_6H_3)N{=}C(CH_3)C(CH_3){=}N(2,6\text{-}Me\text{-}C_6H_3)\}]$ (**2-dab**) were prepared as reported in the literature.[9,25] All experimental manipulations were carried out under nitrogen using Schlenk techniques.

Preparation of $[MoBr(\eta^3\text{-}C_3H_5)(CO)_2\{(C_5H_4N)NH(C_5H_4N)\}]$ (1-adp): Di(2-pyridyl)amine (**adp**) (1.5 mmol, 0.257 g) was added to a yellow solution of $[MoBr(\eta^3\text{-}C_3H_5)(CO)_2(CH_3CN)_2]$ (1.0 mmol, 0.355 g) in ethanol (10 mL) and N_2 whilst stirring. The stirring was continued overnight. The yellow precipitate was filtered off, washed with 3 × 10 mL of diethyl ether and dried under vacuum. Diffusion of diethyl ether into a dmf solution of the compound afforded crystals suitable for single X-ray diffraction studies. $C_{15}H_{14}BrMoN_3O_2$ (444.14): calcd. C 40.56, H 3.17, N 9.46; found C 40.13, H 3.08, N 9.15. IR (KBr pellets): $\tilde{\nu}$ = 3280 (ν_{N-H}) 1929, 1840 ($\nu_{C\equiv O}$), 1634, 1583 (**adp** ring stretches) cm^{-1}. ^1H NMR ([D$_7$]DMF, 233 K), **isomer A** (69%): δ = 10.86 (s, 1 H, N*H*), 8.37 (d, $^3J_{H^6-H^5}$ = 5.6 Hz, 2 H, H^6), 7.87 (t, ^3J = 8 Hz, 2 H, H^4), 7.24 (d, $^3J_{H^3-H^4}$ = 8.4 Hz, 2 H, H^3), 7.12 (t, ^3J = 6.4 Hz, 2 H, H^5), 4.05 (m, 1 H, H^{meso}), 2.44 (d, $^3J_{H^{syn}-H^{meso}}$ = 6.1 Hz, 2 H, H^{syn}), 1.14 (d, $^3J_{H^{anti}-H^{meso}}$ = 8.8 Hz, 2 H, H^{anti}) ppm. ^{13}C NMR ([D$_7$]DMF, 233 K), **isomer A**: δ = 154.46 (C^6), 153.70 (C^2), 141.06 (C^4), 118.92 (C^5), 115.60 (C^3), 68.35 (C^{meso}), 54.62 ($C^{anti/syn}$). **Isomer B** (24%): 11.18 (s, 1 H, N*H*); [8.83 (d, 1 H), 8.34 and 8.00 (overlapped), 7.95 (t, 1 H), 7.87 (overlapped), 7.54 (d, 1 H), 7.42 (t, 1 H), 7.36 (d, 1 H)], adp rings; 4.16 (m, 1 H, H^{meso}); 3.85 (br., 1 H, H^{syn}); 2.44 (overlapped, H^{syn}); 1.22 (m, 2 H, H^{anti}). **Isomer C** (7%): 11.36 (s, 1 H, N*H*); [8.58 (d, 1 H), 8.34 (overlapped), 8.10 (t, 1 H), 8.00 (overlapped), 7.71 (d, 1 H), 7.54, 7.45 (t) and 7.28 (t) overlapped], adp rings; 4.16 (m, 1 H, H^{meso}), 3.85 (br., 1 H, H^{syn}), 2.44 (overlapped, H^{syn}), 1.22 (m, 2 H, H^{anti}) ppm. (*Note:* % isomers is based on integration ratio of ^1H NMR spectrum at 233 K.)

PILC and PCH Supports: The aluminium pillared natural clay (PILC) was prepared using natural Portuguese clay collected from Porto Santo, Madeira archipelago (denoted as PTS). The structural formula of the Porto Santo clay was $[(Ca_{/2},K,Na)_{0.39}(Al_{1.16},Mg_{0.45},Fe_{0.51})(Si_{3.70},Al_{0.30})O_{10}(OH)_2]$. The pillaring method was optimised to produce pillars based on aluminium oxides by exchanging the cations of the clay with an oligomeric solution made from $AlCl_3$ and NaOH, followed by calcination.[1] The pillars act as spacers creating cavities running along two dimensions. IR (KBr) $\tilde{\nu}$ = 3640, 3465 (vs, br. d), 1648 (m), 1247 (vs), 1052 (vs) cm^{-1}. ^{29}Si MAS NMR: δ = –94.1 (Q^3) ppm. ^{27}Al MAS NMR: δ = 61.3, 3.9 ppm.

The porous clay heterostructure (PCH) was prepared as previously reported[3,4,15] from PTS to be used as a support for comparison

purposes. The clay gallery was opened up by stirring, overnight at 323 K, a suspension of clay (1 g in 100 mL of water) with a solution of ionic surfactant, cetyltrimethylammonium bromide (0.5 M). The air-dried, ion-exchanged clay was then stirred overnight with tetraethylorthosilicate (98%) in the presence of a neutral amine (octylamine, 99%) as cosurfactant. The surfactant template was removed by calcination at 813 K for 6 h. IR (KBr): $\tilde{\nu}$ = 3443 (vs, br. d), 1632 (m), 1240 (s), 1052 (vs), 948 (s), 797 (m), 466 (m) cm^{-1}. ^{29}Si MAS NMR: δ = –91 (Q^2), –99 (Q^3), –107.3 (Q^4) ppm.

Introduction of Mo^{II} Complexes in the Clay Structures: PILC/**1** and PILC/**2**: PILC (500 mg) was impregnated with a solution (10 mL) of **1** (76 mg) or **2** (71 mg) in acetonitrile and stirred for 48 h at room temperature. The solids were filtered, washed three times with acetonitrile and dried in vacuo.

PILC/1: Found C 5.75, N 1.95, Mo 1.4. Selected IR (KBr): $\tilde{\nu}$ = 1934 (w), 1830 (w) cm^{-1}. ^{29}Si MAS NMR: δ = –94.1 (Q^3) ppm. ^{27}Al MAS NMR: δ = 61.7, 3.9 ppm. ^{13}C CP MAS NMR: not observed.

PILC/2: Found C 4.14, N 1.65, Mo 1.4. Selected IR (KBr): $\tilde{\nu}$ = 1937 (w), 1834 (w) cm^{-1}. ^{29}Si MAS NMR: δ = –94.2 (Q^3) ppm. ^{27}Al MAS NMR: δ = 59.9, 3.0 ppm. ^{13}C CP MAS NMR: not observed.

The PILC/**1-adp** and PILC/**2-adp** materials were prepared by adding a solution of acetonitrile (10 mL) containing either **1** (53 mg) (for PILC/**1**) or **2** (50 mg) (for PILC/**2**) to PILC (350 mg). After stirring for 40 h at room temperature, under nitrogen, **adp** (35 mg or 37 mg for PILC/**1-adp** and PILC/**2-adp**, respectively) was added and the resulting mixture was stirred for 54 h. The solid material was filtered, washed with acetonitrile (10 mL) (three times) and dried under vacuum. The PILC/**2-dab** material was prepared in a similar fashion using **dab** (57 mg) instead of **adp**.

PILC/1-adp: Found C 5.04, N 1.55, Mo 2.25. Selected IR (KBr): $\tilde{\nu}$ = 1929 (s), 1839 (s) cm^{-1}. ^{13}C CP MAS NMR: δ = 56 ($C^{allyl–anti/syn}$), 69 ($C^{allyl–meso}$), 110–130 and 140 ($C^{arom.}$), 153 (*C*-NH), 225 (*C*≡O) ppm. ^{29}Si MAS NMR: δ = –94.2 (Q^3) ppm.

PILC/2-adp: Found C 6.43, N 1.90, Mo 2.68. Selected IR (KBr): $\tilde{\nu}$ = 1926 (s), 1840 (s) cm^{-1}. ^{13}C CP MAS NMR: δ = 52 ($C_{allyl–anti/syn}$), 66 ($C_{allyl–meso}$), 105–124 and 137 ($C_{arom.}$), 149 (*C*-NH), 222 (*C*≡O) ppm. ^{29}Si MAS NMR: δ = –94.2 (Q^3) ppm.

PILC/2-dab: Found C 3.45, N 0.19, Mo 0.80. Selected IR (KBr): $\tilde{\nu}$ = 1953 (vw), 1868 (vw) cm^{-1}. ^{13}C CP MAS NMR: δ = 25 (CH_3), 129 (Ph), 161 (N=*C*), 229 (*C*≡O) ppm. ^{29}Si MAS NMR: δ = –94.2 (Q^3) ppm.

PCH/**1-adp** was prepared following the procedure described for the modified PILCs, using PCH (300 mg), a solution of **1** (53 mg) in acetonitrile (10 mL) and **adp** ligand (37 mg). Found C 6.97, N 1.83, Mo 2.55. Selected IR (KBr): $\tilde{\nu}$ = 1930 (s), 1843 (s) cm^{-1}. ^{13}C CP MAS NMR: δ = 56 ($C^{allyl–anti/syn}$), 69 ($C^{allyl–meso}$), 110–126 and 140 (Ph), 153 (*C*-NH), 225 (*C*≡O) ppm. ^{29}Si MAS NMR: δ = –93.9 (Q^3), –104, –111, –113 (Q^4) ppm.

Characterisation: Infrared spectra were measured on a Mattson 7000 FT spectrometer. Samples were run as KBr pellets. ^1H NMR spectra were recorded with a Bruker Avance-400 spectrometer using $CDCl_3$ or [D_7]DMF as solvent. ^1H NMR spectra of 1-adp were obtained at several temperatures between 295 and 233 K. Phase-sensitive NOESY with a mixing time of 1.5 s, COSY and ^{13}C spectra were recorded at 233 K. Microanalyses (C, H and N) were measured by elemental analysis service at ITQB or at the University of Aveiro. Mo was determined by ICP-AES at the Central Laboratory for Analysis, University of Aveiro. Powder XRD data were collected with oriented mounts on a Rigaku diffractometer with Cu-K_α radiation filtered by Ni. ^{29}Si, ^{27}Al and ^{13}C solid-state NMR spectra were recorded at 79.49, 104.26 and 100.62 MHz, respectively, on a (9.4-T) Bruker Avance 400P spectrometer. ^{29}Si MAS NMR spectra were recorded with 40° pulses, spinning rates 5.0–5.5 kHz and 60-s recycle delays. ^{29}Si CP MAS NMR spectra were recorded with 4-μs 1H 90° pulses, 8 ms contact time, a spinning rate of 5 kHz and 4-s recycle delays. For ^{27}Al MAS NMR spectra a 0.6-μs 1π/18 pulse was used with an interpulse delay of 0.2 s. ^{13}C CP MAS NMR spectra were recorded with 4.5-μs ^1H 90° pulses, 2 ms contact time, a spinning rate of 7 kHz and 4-s recycle delays. Chemical shifts are quoted in ppm from TMS. ^{13}C spectra were also recorded in the solid state at 125.76 MHz with a Bruker Avance 500 spectrometer. Nitrogen adsorption–desorption isotherms at 77 K were measured either using a conventional volumetric apparatus with a calibrated Baratron pressure transducer, or an automated Quantachrome (NOVA 1200e) apparatus. The samples were pretreated by degassing at 423 K under vacuum. The specific surface area was estimated for p/p^0 values until 0.15. Microporous volumes were determined from *t*-plots and the mesoporous volumes were obtained subtracting the microporous volume from the total pore volume (adsorbed amount at p/p^0 = 0.95).

X-ray Structure Determination of [$MoBr(CO)_2(\eta^3$-$C_3H_5)$(adp)] (1)

Crystal Data: $C_{15}H_{14}BrMoN_3O_2$, M_r = 444.14; monoclinic space group $P2_1/n$, Z = 4, a = 7.646(9), b = 12.402(14), c = 17.760(21) Å, β = 100.50(1)°, U = 1655.9 $Å^3$, ρ_{calcd} = 1.782 $Mg\,m^{-3}$, (Mo-K_α) = 3.214 mm^{-1}.

X-ray data were collected at room temperature on an MAR research Image plate system using graphite-monochromated Mo-K_α radiation (λ = 0.71073 Å) at Reading University. The crystals were positioned 50 mm from the detector and the frames were measured using an appropriated counting. Data analysis was carried out with the XDS program.[26] An empirical absorption correction was carried out using the DIFABS program.[27]

A total of 8303 reflections were collected and were merged to give 3159 unique reflections with a R_{int} of 0.0905.

The structure was solved by direct methods and subsequent difference Fourier syntheses and refined by full-matrix least-squares on F^2 using the SHELX-97 system programs.[28]

Anisotropic thermal parameters were used for all non-hydrogen atoms. The atomic position of the hydrogen atom of the N–H group was retrieved from a final difference Fourier map. The hydrogen atoms bonded to carbon atoms were included in the refinement in calculated positions. All hydrogen atoms were given thermal parameters equivalent to 1.2 times those of the atom to which they were attached, except the hydrogen atom of the N–H group, which was refined with an individual isotropic temperature factor. The residual electronic density ranged from –0.86 to 1.43 $e\,Å^{-3}$, with the highest peak at 1.0 Å from the molybdenum centre. The final refinement of 203 parameters converged to R^1 = 0.0638, wR_2 = 0.1233 for 2144 reflections with $I > 2\sigma(I)$ and R_1 = 0.1071, wR_2 = 0.1358 for the 3159 unique *hkl* data. Molecular diagrams were drawn with PLA.[29]

CCDC-212399 (for **1**) contains supplementary crystallographic data. These data can be obtained free of charge from The Cambridge Crystallographic Data Centre via www.ccdc.cam.ac.uk/data_request/cif.

Catalysis: The liquid-phase epoxidation of cyclooctene was carried out at 328 K under air (atmospheric pressure) in a micro reaction vessel equipped with a magnetic stirrer and immersed in a thermostatted oil bath, which was loaded with 100 mg of clay-supported catalyst (or of free complex in an amount of Mo equivalent to that

present in the corresponding supported complexes that is initially charged to the reactor), *cis*-cyclooctene (3.6 mmol) and *tert*-butyl hydroperoxide (5.5 mmol, 5.5 M in decane). Samples were withdrawn periodically and analysed using a gas chromatograph (Varian 3800) equipped with a capillary column (SPB-5, 20 m × 0.25 mm × 0.25 μm) and a flame ionisation detector. Undecane was used as an internal standard added after the reaction. The stability of the supported catalysts was investigated by carrying out a second 24-h run with the recovered solid. Prior to reuse the solid was separated from the reaction solution by centrifugation, washed with *n*-hexane and dried at room temperature overnight. The stability of the homogeneous catalysts was investigated by recharging the micro reactor, at 24 h, with olefin and oxidant in identical amounts to those used initially in the first run and stirring the solution for a further 24 h.

Acknowledgments

The authors are grateful to Fundação para a Ciência e a Tecnologia (FCT) and Programa Operacional Ciência, Tecnologia, Inovação (POCTI) for financial support (POCTI/QUI/44654/2002). S. Q. and P. P. acknowledge FCT for fellowships (SRFH/BPD/11463/2002 and SFRH/BD/1166/2000). P. N. is grateful to CICECO-University of Aveiro for a research grant. We thank EPSRC and the University of Reading for funds for the Image Plate system.

[1] M. B. Carvalho, J. Pires, A. P. Carvalho, *Microporous Mater.* **1996**, *6*, 65–77.
[2] A. Gil, L. M. Gandía, M. A. Vicente, *Catal. Rev. Sci. Eng.* **2000**, *42*, 145–212.
[3] A. Galarneau, A. Barodawalla, T. J. Pinnavaia, *Nature* **1995**, *374*, 529–531.
[4] M. Polverejan, Y. Liu, T. J. Pinnavaia, *Chem. Mater.* **2002**, *14*, 2283–2288.
[5] A. P. Carvalho, C. Castanheira, B. Cardoso, J. Pires, A. R. Silva, C. Freire, B. de Castro, M. B. Carvalho, *J. Mater. Chem.* **2004**, *14*, 374–379.
[6] B. Cardoso, J. Pires, A. P. Carvalho, M. B. Carvalho, I. Kuźniarska-Biernacka, A. R. Silva, C. Freire, B. de Castro, *Eur. J. Inorg. Chem.* **2005**, 837–844.
[7] I. Kuźniarska-Biernacka, A. R. Silva, R. Ferreira, A. P. Carvalho, J. Pires, M. B. Carvalho, C. Freire, B. de Castro, *New J. Chem.* **2004**, *28*, 853–858.
[8] P. Das, I. Kuźniarska-Biernacka, A. R. Silva, A. P. Carvalho, J. Pires, C. Freire, *J. Mol. Catal. A* **2006**, *248*, 135–143.
[9] J. C. Alonso, P. Neves, M. J. P. Silva, S. Quintal, P. D. Vaz, C. Silva, A. A. Valente, P. Ferreira, M. J. Calhorda, V. Félix, M. G. B. Drew, *Organometallics* **2007**, *26*, 5548–5556.
[10] R. A. Howie, G. Izquierdo, G. P. McQuillan, *Inorg. Chim. Acta* **1983**, *72*, 165.
[11] J. R. Ascenso, C. G. Azevedo, M. J. Calhorda, M. A. A. F. de C. T. Carrondo, P. Costa, A. R. Dias, M. G. B. Drew, V. Félix, A. M. Galvão, C. C. Romão, *J. Organomet. Chem.* **2001**, *632*, 197–208.
[12] P. M. F. J. Costa, M. Mora, M. J. Calhorda, V. Félix, P. Ferreira, M. G. B. Drew, H. Wadepohl, *J. Organomet. Chem.* **2003**, *687*, 57–68.
[13] S. Trofimenko, *Inorg. Chem.* **1970**, *11*, 2493–2499.
[14] D. R. Van Staveren, E. Bill, E. Bothe, M. Bühl, T. Weyhermüller, N. Metzler-Nolte, *Chem. Eur. J.* **2002**, *8*, 1649–1662.
[15] J. Pires, A. C. Araújo, A. P. Carvalho, M. L. Pinto, J. M. González-Calbet, J. Ramírez-Castellanos, *Microporous Mesoporous Mater.* **2004**, *73*, 175–180.
[16] C. Freund, M. Abrantes, F. E. Kühn, *J. Organomet. Chem.* **2006**, *691*, 3718–3729.
[17] A. A. Valente, J. D. Seixas, I. S. Gonçalves, M. Abrantes, M. Pillinger, C. C. Romão, *Catal. Lett.* **2005**, *101*, 127–130.
[18] P. Ferreira, I. S. Gonçalves, F. E. Kühn, A. D. Lopes, M. A. Martins, M. Pillinger, A. Pina, J. Rocha, C. C. Romão, A. M. Santos, T. M. Santos, A. A. Valente, *Eur. J. Inorg. Chem.* **2000**, 2263–2270.
[19] Z. Petrovski, M. Pillinger, A. A. Valente, I. S. Gonçalves, A. Hazell, C. C. Romão, *J. Mol. Catal. A* **2005**, *227*, 67–73.
[20] A. Al-Ajlouni, A. A. Valente, C. D. Nunes, M. Pillinger, A. M. Santos, J. Zhao, C. C. Romão, I. S. Gonçalves, F. E. Kühn, *Eur. J. Inorg. Chem.* **2005**, 1716–1723.
[21] F. E. Kühn, M. Groarke, E. Bencze, E. Herdtweck, A. Prazeres, A. M. Santos, M. J. Calhorda, C. C. Romão, I. S. Gonçalves, A. D. Lopes, M. Pillinger, *Chem. Eur. J.* **2002**, *8*, 2370–2383.
[22] C. D. Nunes, A. A. Valente, M. Pillinger, J. Rocha, I. S. Gonçalves, *Chem. Eur. J.* **2003**, *9*, 4380–4390.
[23] C. D. Nunes, M. Pillinger, A. A. Valente, J. Rocha, A. D. Lopes, I. S. Gonçalves, *Eur. J. Inorg. Chem.* **2003**, 3870–3877.
[24] M. J. Schadt, N. J. Gresalfi, A. J. Lees, *Inorg. Chem.* **1985**, *24*, 2942–2946.
[25] H. T. Dieck, H. Friedel, *J. Organomet. Chem.* **1968**, *14*, 375–385.
[26] W. J. Kabsch, *J. Appl. Crystallogr.* **1988**, *21*, 916.
[27] DIFABS: N. Walker, D. Stuart, *Acta Crystallogr., Sect. A* **1983**, *39*, 158–166.
[28] G. M. Sheldrick, *SHELX-97*, University of Göttingen, Göttingen, **1997**.
[29] A. L. Spek, *PLATON, A Multipurpose Crystallographic Tool*, Utrecht University, Utrecht, The Netherlands, **1999**.

Received: September 7, 2007
Published Online: January 7, 2008

